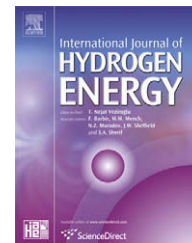


Available at www.sciencedirect.comjournal homepage: www.elsevier.com/locate/he

Technical Communication

Analysis of battery backup and switching controller for a fuel-cell powered automobile

Panini Kolavennu^a, John C. Telotte^a, Srinivas Palanki^{b,*}

^aDepartment of Chemical and Biomedical Engineering, FAMU-FSU College of Engineering, Florida State University, 2525 Pottsdamer Street, Tallahassee, FL 32310-6046, USA

^bDepartment of Chemical Engineering, University of South Alabama, 307 University Boulevard North, Mobile, AL 36688-0002, USA

ARTICLE INFO

Article history:

Received 23 October 2007

Received in revised form

13 August 2008

Accepted 18 September 2008

Available online 18 November 2008

Keywords:

Fuel cell

Battery backup

Automobile

ABSTRACT

In this paper, we consider the design of a fuel-cell powered automobile that utilizes methane as a source of hydrogen to power a PEM fuel cell. It is shown that when the power demand of the motor goes up suddenly, there is a time lag for generating the necessary hydrogen. A battery backup that provides the necessary power during this time lag is analyzed via an equivalent circuit model. A logic-based switching controller that switches between the fuel cell and the backup battery is designed to meet the power demand. The efficacy of this scheme is tested via simulations on a power profile obtained from a realistic speed profile of a small automobile.

© 2008 International Association for Hydrogen Energy. Published by Elsevier Ltd. All rights reserved.

1. Introduction

Fuel-cell power systems for automotive applications have received increased attention in recent years because of their potential for high fuel efficiency and lower emissions [1]. In particular, a fuel cell converts hydrogen and oxygen into water, directly generating electrical energy from chemical energy without being restricted by efficiency limits of the Carnot thermal cycle [2]. This interest in automotive applications has primarily been the result of the breakthroughs made in polymer electrolyte membrane (PEM) fuel cells which have several attractive features such as low operating temperatures (around 80 °C), relatively low cost, simple maintenance requirements, and high efficiency. There are several recent articles that address several issues specific to the use of fuel-cell technology to automotive applications,

such as life cycle assessment of fuel cells [3] and system efficiency [4].

While there have been significant advances in fuel-cell technology, one reason this technology has not seen widespread applications in the automotive industry has been the lack of an efficient hydrogen distribution center and the difficulties associated with storing hydrogen onboard an automobile [5]. One option to alleviate these problems is to develop a system that utilizes a commonly available carbon-based hydrogenous fuel such as gasoline or methane to generate the necessary hydrogen *in situ* on an “as needed” basis [6,7]. Hydrocarbon fuels are relatively easy to store onboard a vehicle and a nationwide infrastructure to supply these fuels already exists.

In an earlier paper [8], the primary components of a fuel-cell power system, that utilizes methane to generate hydrogen, were analyzed. In particular, basic chemical

* Corresponding author.

E-mail address: spalanki@usouthal.edu (S. Palanki).

Nomenclature

A	area, cm^2
C_{A0}	concentration of the gas, moles/l
F	Faraday's constant
F_{H_2}	flow rate of Hydrogen, mol/min
F_{CH_4}	flow rate of Methane, mol/min
i	current density, A/cm^2
I	current, A
N	number of cells in the stack
R_b	internal Resistance of the battery
P	power, w
SOC	state of charge
V	voltage, V
V_{oc}	open-circuit voltage, V
V_{term}	battery terminal voltage, V
V_r	volume of the reactor, l
X	conversion of hydrogen in the fuel cell
τ	space time, s

engineering principles were utilized to design a reactor train that converts methane to hydrogen of the desired purity. The relation between power produced by a PEM fuel cell and methane entering the reactor train at steady state was calculated. However, a typical automobile does not operate at steady state. The power demand for an automobile motor undergoes significant variations due to acceleration, changes in road surface and traffic conditions. While it is straightforward to handle reduction in power demand, a sudden increase in power demand requires an instantaneous increase in hydrogen flow rate into the fuel cell. However, the conversion of methane to hydrogen takes several seconds which leads to an unacceptable lag between power demand of the motor and the power supplied by the fuel cell. In this paper, a backup battery is analyzed that takes over this power load during the

time it takes for the fuel cell to generate the necessary power. A switching controller is designed that switches to the battery backup till the fuel cell is able to generate the necessary power. This system is tested via simulations for a typical power profile of an automobile motor.

2. System design considerations

A schematic of the fuel-cell system under consideration is shown in Fig. 1. The two main components of the overall system are (1) the fuel processing subsystem and (2) the power generation subsystem. Methane enters the fuel processing subsystem and is converted to hydrogen. Hydrogen enters the fuel cell where it reacts with oxygen to generate electrical power which drives an electric motor.

In addition to the fuel cell, there is a battery backup that the electric motor switches to when the hydrogen delivered to the fuel cell is insufficient to meet the instantaneous power demands of the electric motor. This battery backup is essential because significant load transitions occur frequently as a result of sudden acceleration on highway ramps as well as terrain changes [1].

In this paper, we consider the design and operation of a fuel-cell system for a rating of 50 kW. This figure may seem low ($50 \text{ kW} = 67 \text{ hp}$) when compared to power ratings of today's internal combustion engines; yet because electric motors deliver maximum torque at all rpms while internal combustion engines deliver maximum torque only at an optimal rpm. Thus internal combustion engines operate at a fraction of their nominal power rating while electric motors operate at their rated power at all times [1].

2.1. Fuel processing subsystem

In this subsystem, methane is converted to hydrogen. In a previous publication [8], we utilized basic chemical

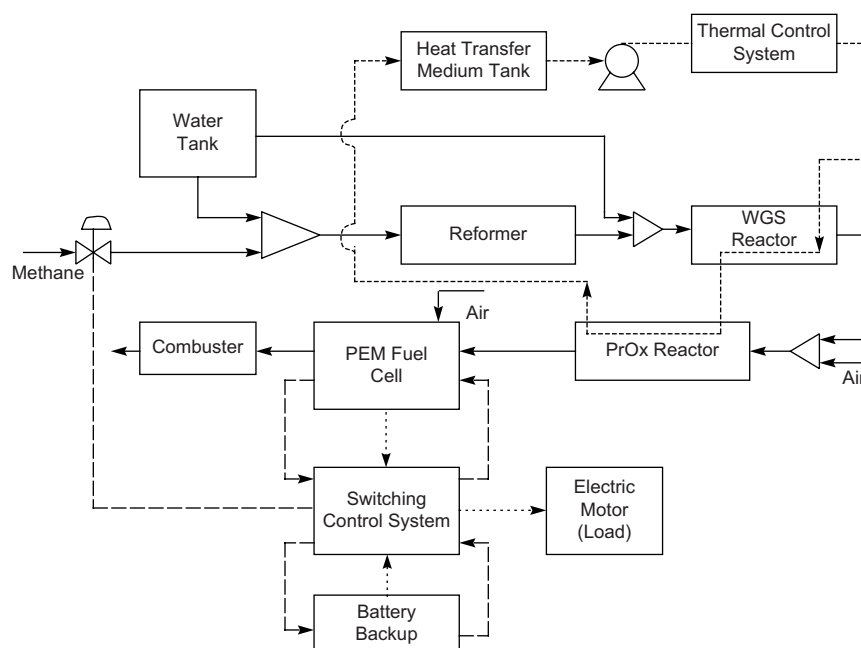


Fig. 1 – Schematic of fuel-cell system.

engineering principles to design a reactor train that produced hydrogen of the desired purity. The design operating conditions of this series of reactors are summarized in Table 1.

The steam reformer operates at 1000 K and 5 atm and utilizes a steam to carbon ratio of 3:1. The water-gas shift reactor operates at 2 atm and has two temperature zones. The initial 1 l is operated at 700 K (HT) to promote high reaction rate and the remaining 40.8 l are operated at 490 K (LT) to promote high conversion. The preferential oxidation reactor operates at 473 K and 2 atm. It was shown [8] that the relation between methane utilized and hydrogen produced was linear and could be represented by the following relation:

$$F_{H_2} = 3.12F_{CH_4} \quad (1)$$

2.2. Design of power generation subsystem

The current generated by the fuel-cell stack is directly proportional to the hydrogen consumption rate. The voltage generated by a cell depends on the current density in the cell, thermodynamic parameters (temperature and partial pressures) and the cell materials and design. For a given cell design and thermodynamic state a detailed calculation of the voltage versus current density can be performed. In a previous publication [8], we utilized a semi-theoretical model first proposed by Larminie and Dicks [2] and later parameterized by Pukrushpan [9]. For a fuel cell operating at 353 K with an anode partial pressure of hydrogen of 3 bar and air fed to the cathode at 5 bar, the following cell polarization curve is obtained:

$$V = 0.6405 + 0.3325e^{-10i} - 0.03036i - 0.00355i^3 \quad (2)$$

This relation is plotted in Fig. 2. It should be noted that for these conditions there is a sharp drop-off in cell voltage at small current densities but a very flat region to the polarization curve with cell voltages being nearly 0.6 V over a wide range of current densities. This is desirable characteristic as this produces a power density that varies nearly linearly with current density, as seen in Fig. 3.

The design objective for this project has been for a 50 kW fuel-cell stack. We have based our design on a cell voltage of 0.6 V. This occurs for a current density of 1.15 A/cm². If one desires a system with a 300 V output [9], then 500 cells in series are required. To generate 50 kW of power, 166.67 A of current is required which requires an active cell area of 145 cm². The required hydrogen flow per cell is calculate from

$$I = 2FXF_{H_2} \quad (3)$$

The conversion is assumed to be 90%, which yields a maximum required hydrogen flow of 0.001 moles/sec/cell. This corresponds to a total required methane flow of 9.2 moles/min. The power curve for the combined fuel processor and fuel-cell stack system is shown in Fig. 4. To construct this curve a methane flow rate was selected and the resultant hydrogen flow from the fuel processor was calculated using equation (1). Using equation (3), the cell current was then determined. With the cell area specified at 145 cm², the current density could then be found and the stack power was finally calculated using equation (2).

2.3. Dynamic system interaction

When the power demand increases suddenly (e.g. due to sudden acceleration), an instantaneous increase in hydrogen is required. However, since it takes time for reactants and products to go through the reactor train, there is a time delay in producing the hydrogen. If the reactions are not kinetically limited, this time delay can be estimated from the space time of the reactor train. The space time of a plug flow reactor is given by

$$\tau = \frac{F_{A0}}{C_{A0}} \quad (4)$$

where τ is the space time, F_{A0} is the molar flow rate and C_{A0} is the concentration of component A entering the reactor. During this time delay, it is necessary to have a battery backup that provides the necessary power to the motor while the reactor train generates the necessary hydrogen.

Clearly, the space time changes if the inlet flow of reactants change. We designed the reactors for a maximum flow rate of methane of 10 mol/min. For this flow rate the volume and the space time for each of the reactor is given in Table 2. It is observed that there can be up to a 4 s delay in generating the necessary hydrogen.

In the next section, a battery backup is analyzed that provides the maximum power that the automobile needs for at least 4 s. This time is sufficient for the fuel processing system to generate the necessary hydrogen for the fuel cell.

3. Battery modeling

There has been considerable research effort in modeling fuel cells [10,11]. In electric and fuel-cell vehicles the battery is charged and discharged continuously and so knowledge of the transient behavior of the batteries is very important. Dynamic models developed from electrochemical principles like the

Table 1 – Fuel processing subsystem.

Reactor name	Reactions	Temperature (K)	Pressure (atm)	Size (l)
Steam reformer	CH ₄ + H ₂ O ⇌ 3H ₂ + CO CO + H ₂ O ⇌ CO ₂ + H ₂ CH ₄ + 2H ₂ O ⇌ 4H ₂ + CO ₂	1000	5	10
Water-gas shift	CO + H ₂ O ⇌ CO ₂ + H ₂	700 (high temp.) 490 (low temp.)	2	41.8
Preferential oxidation	CO + (1/2)O ₂ ⇌ CO ₂ H ₂ + (1/2)O ₂ ⇌ H ₂ O	473	2	0.35

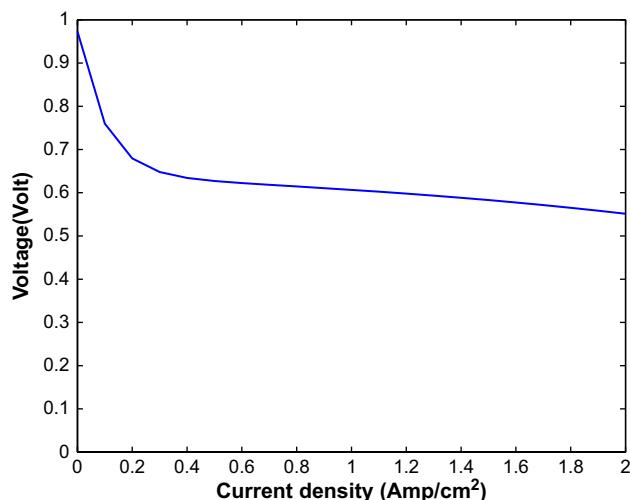


Fig. 2 – Polarization curve.

cell sandwich model [12] give spatial distribution of potentials and chemical compositions inside the cell as well as the transient behavior of cell potential and temperature. However for control oriented studies we require models which can be simulated quickly. Equivalent electric circuit models have been developed in the literature which give an accurate prediction of state of charge (SOC) of the battery [13].

He and Hodgson [13] have observed that while discharging a battery over a period of time there exists a cutoff or critical voltage beyond which the battery performance deteriorates rapidly as the voltage begins to fall rapidly. To avoid operation near the critical voltage the state of charge is set to zero at the cutoff voltage and is defined as

$$\text{SOC} = 1 - \frac{V_{\text{oc}_{\text{cutoff}}}}{V_{\text{oc}_{\text{full}}}} \quad (5)$$

where $V_{\text{oc}_{\text{full}}}$ is the voltage of the battery at full capacity and $V_{\text{oc}_{\text{cutoff}}}$ is the battery terminal voltage at the critical point. Practically, it is difficult to measure the open-circuit voltage at each instant hence utilizing the relationship between the SOC and the available battery capacity SOC can be redefined as

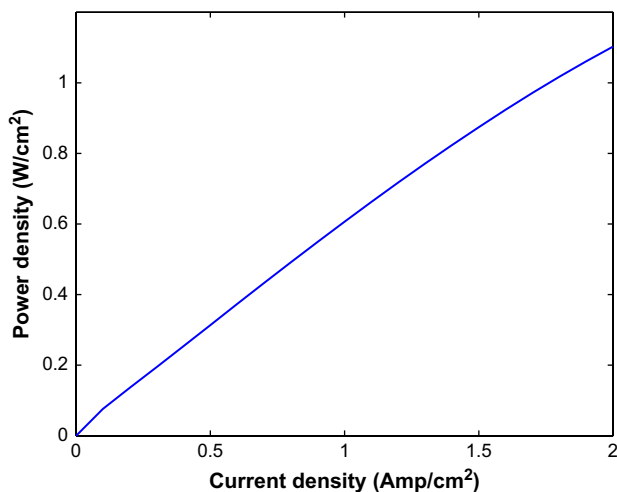


Fig. 3 – Power density vs. current density.

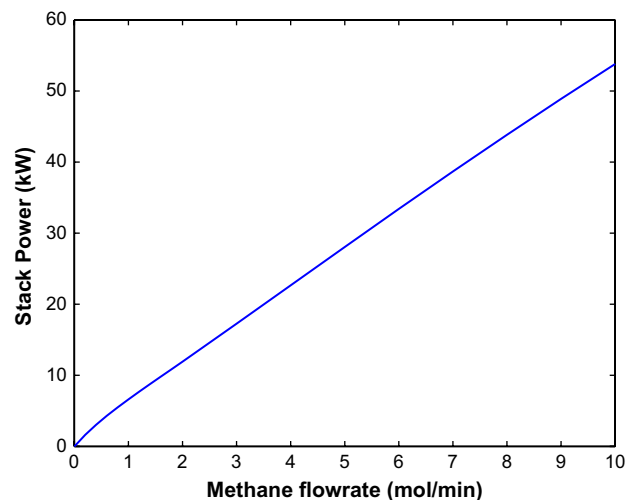


Fig. 4 – Effect of methane flow on power generated.

$$\text{SOC} = 1 - \frac{\text{Used capacity}}{\text{Total capacity}} \quad (6)$$

The total current drawn from the battery can be used as an indicator for the used capacity and is given by.

$$\text{CAP}_{\text{used}} = \int_0^t I \cdot dt \quad (7)$$

So now the SOC is one when the battery is fully charged and zero when discharged to the critical voltage. It is desirable to maintain the SOC around 0.5–0.7.

A battery model which requires experimentally obtained open-circuit voltage and battery resistance data and predicts the battery terminal voltage, current, and SOC as a dynamic function of operator imposed power demand has been developed based on the model by He and Hodgson, [13]. The model consists of the battery as an ideal voltage source with an internal resistance. This battery model is characterized by the idealized open-circuit voltage, V_{oc} , and the internal battery resistance, R_b . The terminal voltage can be expressed in terms of V_{oc} and R_b as

$$V_{\text{term}} = V_{\text{oc}} - I \times R_b \quad (8)$$

The terminal voltage of a battery during discharge is lower than the instantaneous open-circuit voltage because of the internal resistance inside the battery. Hence current I is given a positive sign when the cell is discharging. Similarly when the cell is charging we need to apply a voltage greater than the V_{oc} to overcome the internal resistance inside the cell so the current in this case is chosen to be negative.

Table 2 – Space time calculation.

Reactor	Volume (l)	Space time (s)
Reformer	10	0.87
Water-gas shift	41.8	2.16
Preferential oxidation	0.35	0.02
Total	50.5	3.05

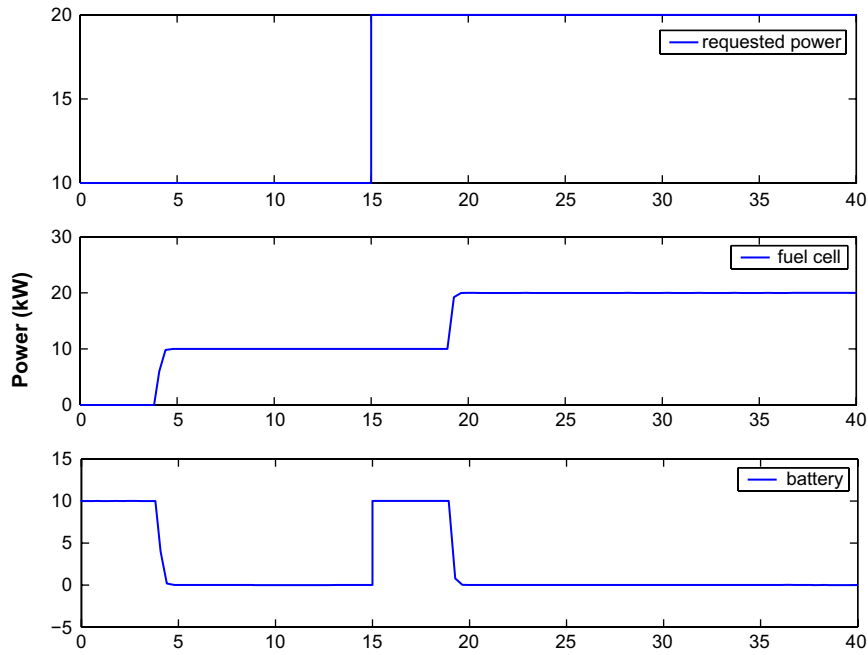


Fig. 5 – Power profile.

The open-circuit voltage and the internal resistance of the battery are both functions of SOC and temperature. For a battery operating at constant temperature the relationship between V_{oc} , R_b and the SOC can be determined experimentally.

The power available at the terminals of the battery is given by the product of voltage and current and substituting the expression for voltage from equation (8), we have

$$P_{wI_{term}} = V_{term}I = IV_{oc} - I^2 \times R_b \tag{9}$$

For a particular power demand we can calculate the current by solving equation (9) which is a quadratic equation in I .

$$I = \frac{V_{oc} - \sqrt{(V_{oc}^2 - 4.R_b.P_{wI_{term}})}}{2R_b} \tag{10}$$

where V_{oc} and R_b are both functions of the SOC. The same sign convention as was used for the current is used i.e. the power is positive during discharge and negative during charge. The current calculated from equation (10) is used to calculate the used capacity from equation (7), which in turn is used to calculate the SOC by equation (6). The V_{oc} and R_b are obtained for the new SOC from the experimental data. Using the new values of V_{oc} and R_b the current is estimated using equation (10).

4. Switching controller

The switching controller is a logic-based on-off controller that switches back and forth between the fuel cell and the battery to meet the power demand. As discussed earlier there is a time lag between the methane entering the reformer and the hydrogen coming out of the fuel processor. If the power demand remains constant the power produced by the fuel cell

is sufficient to meet the power demand. The actual power demand curve is not a straight line and has a lot of fluctuations. To meet this fluctuating power demand, the fuel cell may switch to the battery. The switching controller has to address the following scenarios:

- *Increase in power demand:* Whenever there is an increase in power demand the fuel cell cannot produce the required power (P_r) because of the time delay (τ) in producing power and hence any deficit in power demand is handled by switching to the battery until the fuel cell can produce sufficient power. During this time delay the power produced by the battery is

$$P_{bat} = P_r - P_{fc} \quad \text{for } t < \tau \tag{11}$$

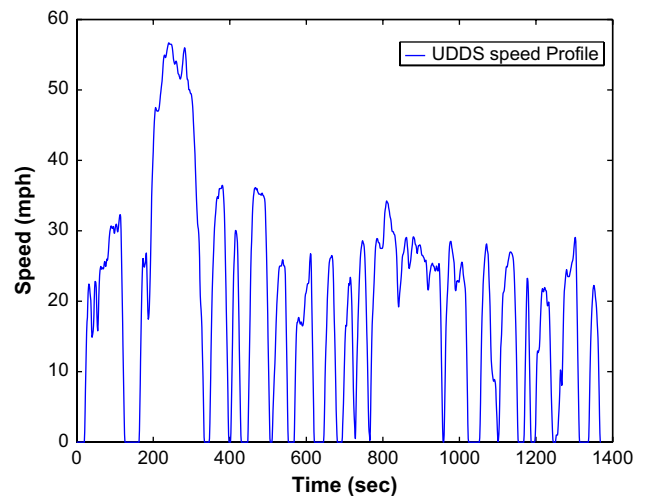


Fig. 6 – Speed vs time profile for UDDS.

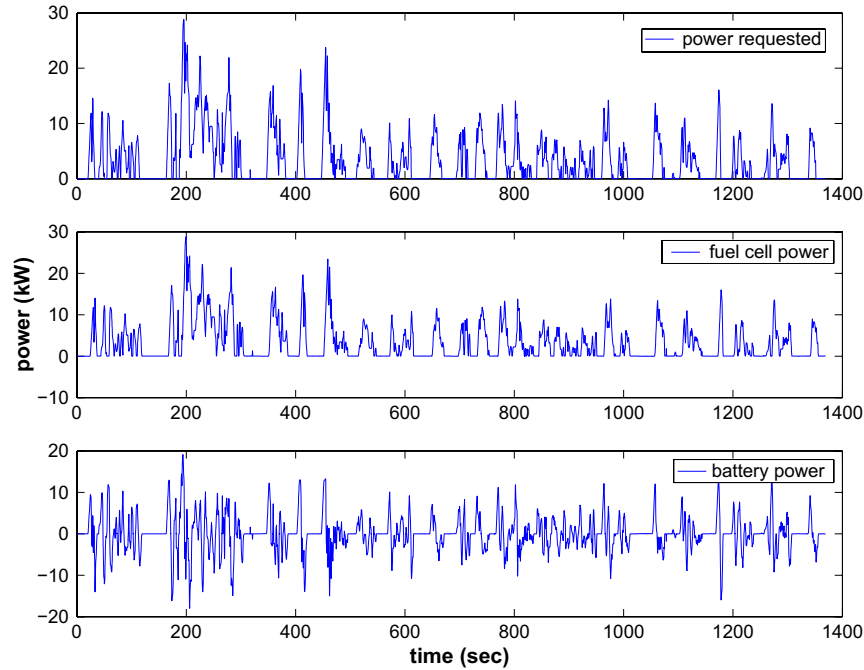


Fig. 7 – Power profiles for the UDDS.

- Decrease in power demand:** During deceleration or decrease in power demand the fuel cell continues to produce the power requested until the time delay has elapsed. This excess power produced by the fuel cell during decrease in power demand should be routed to the battery, so that the battery can be charged. The same equation used in the scenario above can be used here. Since here the power requested is less than the power produced by the fuel cell the P_{bat} is negative which indicates that the battery is being charged.
- State of charge:** The state of charge of the battery should be always maintained above a specified target (SOC_{target}). But during sudden increase in power demand the battery might be discharged rapidly and the SOC might fall below the specified target and also the initial SOC itself might be less than the SOC_{target} . When the SOC of the battery falls below SOC_{target} the controller should direct the fuel cell to produce power to charge the battery in addition to the power demand.

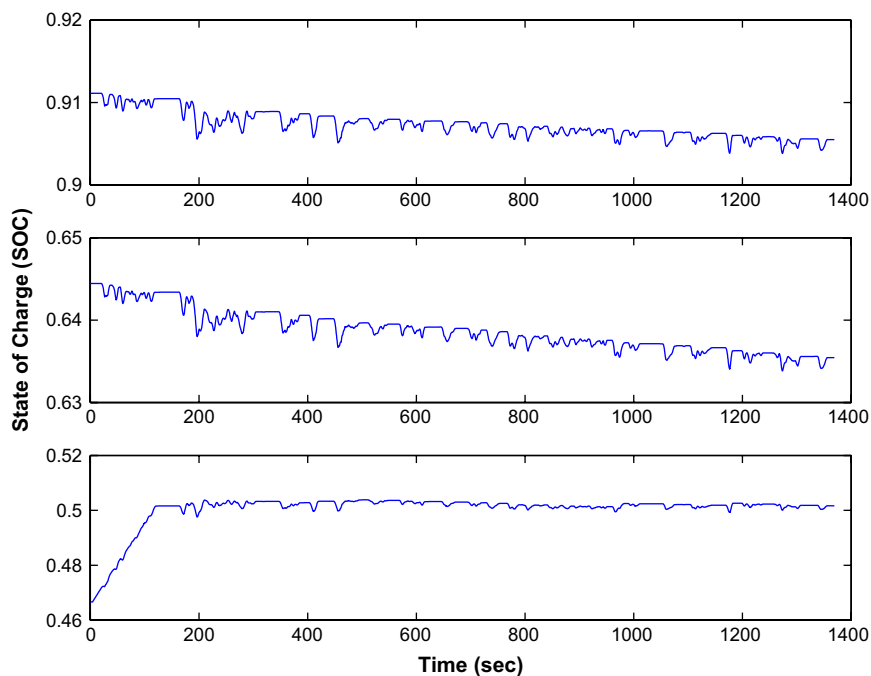


Fig. 8 – State of charge for different initial conditions.

$$P_{fc} = P_r + P_{bat} \quad \text{if } SOC < SOC_{target} \quad (12)$$

- **Total power demand:** Since the fuel processor and the fuel-cell system were designed for a maximum power output of 50 kW, the switching controller should make sure that the power demand from the fuel cell is not greater than 50 kW.

5. Implementation

The fuel processor, fuel-cell system and battery model along with the switching controller were simulated in MATLAB for different power demands. For a simple case where the power demand is a step increase followed by a step decrease the power profiles are given in Fig. 5. Notice that the fuel cell supplies the power with a time delay of 4 s in the meantime the battery supplies the requested power demand. Once the fuel cell is able to meet the power demand the battery is turned off until 15 s at which time the battery again is used to supply the necessary power demand. At 30 s when there is a decrease in power demand the deficit power is sent to the battery to charge it until the fuel cell reaches the level of the new power demand.

To get a more realistic power vs time profile we obtained the power profile for a small car from an existing speed vs time profile using ADVISOR software package [14]. The Urban Dynamometer Driving schedule (UDDS) which is designed for light duty vehicle testing in city driving conditions has been used. The speed versus time profile is shown in Fig. 6. The profiles of power requested, fuel-cell power and battery power versus time are plotted in Fig. 7.

The power supplied by the battery also depends on the initial SOC of the battery. For the same cycle the system was simulated for different initial SOC as shown in Fig. 8. The controller was designed to maintain the SOC above 0.5. For the initial conditions where the battery is almost charged (SOC = 0.9) and semi charged (SOC = 0.64) the profiles look similar. But for the case where the initial SOC is less than 0.5 the controller is activated and brings the SOC level to above 0.5.

6. Discussion and conclusions

In this paper, a battery backup is analyzed for a fuel-cell powered automobile that generates hydrogen *in situ* from methane. The battery is modeled via an equivalent circuit model that tracks the state of charge and power of the battery. A logic-based switching controller is designed that compares the power requested by the motor and the power produced by the fuel cell and switches to the backup battery till the power produced by the fuel cell is sufficient to meet the power demand. A power profile of the motor is obtained from a realistic speed profile of a small automobile and the switching controller is implemented of this profile. It is observed that the switching controller successfully switches to the backup battery when the power demand exceeds the power produced by the fuel cell.

Current battery technology in hybrid vehicles involves the use of nickel metal hydride (NiMH) battery packs. For

instance, the Toyota Prius consists of 38 prismatic modules of a new generation NiMH design with a total pack nominal voltage of 273.6 V and a total energy capacity of 1.8 kWh [15]. The dimensions of this battery pack are 19.6 mm × 106 mm × 275 mm (volume of 57 l). The battery considered in this paper is of the same order of magnitude with a peak voltage of 300 V. If we assume that the energy capacity of the battery is 1.8 kWh (same as the Prius battery) and the battery has to have a state of charge of at least 50%, this battery would deliver 50 kW for 1 min starting from a fully charged state before depleting to 50%. Thus, from a cold start, the reformer would have to be operational within 1 min so that the car can switch from the battery to the fuel cell. It was shown in the previous section that once the fuel cell is operational, under realistic city driving conditions, the charge of the battery never goes under 50%. Newer gas–electric and fuel-cell–electric hybrid vehicles use lithium ion battery technology. These batteries have superior power density versus energy density characteristics when compared to either NiMH batteries or supercapacitors. The second generation Honda Clarity fuel-cell–electric hybrid is equipped with such a battery module. It is rated for 283 V, and replaces the super capacitor energy storage system of the first generation Clarity. Improvement in lithium ion battery technology is ongoing. Current research indicates that energy capacity of 6–18 kWh are achievable with a calendar life of 15 years and 2500–5000 charge depleting cycles [16]. Preliminary research on magnesium ion battery systems suggests that another order of magnitude in performance improvement is achievable [16].

REFERENCES

- [1] Zalc JM, Loffler DG. Fuel processing for PEM fuel cells: transport and kinetic issues of system design. *J Power Sources* 2002;111:58–64.
- [2] Larminie J, Dicks A. *Fuel cell systems*. New York: Wiley; 2000.
- [3] Pei P, Chang Q, Tang T. A quick evaluating method for automotive fuel cell lifecycle. *Int J Hydrogen Energy* 2008; 33(14):3829–36.
- [4] Semelsberger TA, Borup RL. Fuel effects on start-up energy and efficiency for automotive PEM fuel cell systems. *Int J Hydrogen Energy* 2005;30(4):425–35.
- [5] Lovins AB, Williams BD. A strategy for the hydrogen transition. 10th Annual U.S. hydrogen meeting, Vienna, Virginia, April 1999.
- [6] Falco MD. Pd-based membrane steam reformers: a simulation study of reactor performance. *Int J Hydrogen Energy* 2008;33(12):3036–40.
- [7] Bowers BJ, Zhao JL, Ruffo M, Khan R, Dattatraya D, Dushman N, et al. Onboard fuel processor for PEM fuel cell vehicles. *Int J Hydrogen Energy* 2007;32(10–11): 1437–42.
- [8] Kolavennu PK, Telotte JC, Palanki S. Design of a fuel cell power system for automotive applications. *Int J Chem Reactor Eng* 2006;4:A19.
- [9] Pukrushpan JT. Modeling and control of fuel cell systems and fuel processors, PhD thesis, The University of Michigan, Ann Arbor; 2003.
- [10] Nguyen TV, White RE. A water and heat management model for proton-exchange-membrane fuel cells. *J Electrochem Soc* 1993;140(8):2178–86.

-
- [11] Kim J, Lee SM, Srinivasan S. Modeling of proton exchange membrane fuel cell performance with an empirical equation. *J Electrochem Soc* 1995;142(8):2670.
- [12] Doyle M, Meyers JP, Newman J. Computer simulations of the impedance response of lithium rechargeable batteries. *J Electrochem Soc* 2000;147:99–110.
- [13] He X, Hodgson JW. Modeling and simulation for hybrid electric vehicles: modeling. *IEEE Trans Intell Transp Syst* 2002;3:235–43.
- [14] National Renewable Energy Laboratory. ADVISOR (Advanced vehicle simulator); 2002.
- [15] Kelly KJ, Mihalic M, Zolot M. Battery usage and thermal performance of the Toyota Prius and Honda insight during chassis dynamometer testing. NREL/CP-540-31306; 2001.
- [16] Axsen J, Burke A, Kurani K. Batteries for plug-in hybrid electric vehicles (PHEVs): goals and the state of technology circa 2008. UCD-ITS-RR-08-14; 2008.